Mineralogy and Petrology (2002) 76: 247–259

Mineralogy and Petrology

Quantitative cathodoluminescence (CL) spectroscopy of minerals: possibilities and limitations

D. Habermann

Institute of Experimental Physics, University of Technology, Freiberg, Germany

Received December 6, 2001; revised version accepted May 10, 2002
Editorial handling: A. Finch

Summary

The luminescence spectrum of a mineral contains complex information related to the intrinsic crystal and the defect structure. For quantitative analysis of cathodoluminescence (CL) the spectra have to be deconvoluted by fitting and filtering procedures to identify and measure individual peaks. Peak-width, peak-position and transition probability of the luminescence centres are influenced by effects such as interactions within the defects themselves, and interaction between defects and the surrounding crystal lattice. For calcite and feldspar a linear correlation between the defect concentration of manganese and the Mn^{2+}-activated CL-intensity is documented. Combined Micro-Particle Induced X-ray Emission (μ-PIXE) and CL-spectroscopy analyses of REE-doped synthetic calcite suggest a linear correlation between REE-activated CL intensity and REE-concentration at REE-concentration levels below approximately 500 ppm. Sensitising and quenching by other REE are dominant effects yielding strong variations in the correlation between the REE-activated CL-intensity and the REE-content.

Introduction

Since the advent of new CL instrumentation, the cathodoluminescence (CL) of minerals is finding ever-increasing applications in the fields of geoscience, physics and material sciences (e.g. *Richter* and *Zinkernagel*, 1981; *Ramseyer* et al., 1989; *Yacobi* and *Holt*, 1990; *Neuser*, 1995). CL is widely used qualitatively to detect the trace element distribution in minerals. Numerous investigations have examined the possibility of *quantitative* analysis of activator elements by their CL-intensity (e.g. *Frank* et al., 1982; *Mason*, 1987; *Hemming* et al., 1989; *Habermann* et al., 2000). The most important advantages of quantitative CL-spectroscopy compared to

standard in-situ trace element determinations by Electron Probe MicroAnalysis (EPMA) or Particle-Induced X-ray Emission (PIXE) are the combination of high sensitivity, plus the crystal field information obtained regarding the coordination of the activator and its ionic charge. This complexity embedded in the CL-spectra requires them to be decoded fully for the development of quantitative CL-spectroscopy. The improvement of CL as a quantitative analysis method is to be expected when activation, quenching and sensitising mechanisms are well understood and the CL-spectra can be processed by computer software. There are no systems in which a simple linear correlation across the full range of activator concentration exists. However, a linear correlation does exist in special cases (*Hemming* et al., 1989; *Telfer* and *Walker*, 1978; *Habermann* et al., 2000) or can be found in the concentration range of a few to $\sim 10^3$ ppm of activator concentration (*Mason*, 1987; *Habermann*, 1997). This paper presents some of these special cases and results from decoding CL-spectra with special emphasis on REE-activated CL.

Material and methods

The CL-spectra were recorded with a CL-spectrometer attached to a hot cathode CL-microscope (HCLM-1, *Neuser*, 1995) operating at 15 kV accelerating voltage and $\sim 9\,\mu A\,mm^{-2}$ beam current density. To keep the current densities comparable, the stimulation was controlled by spectrometric analyses of the CL intensity using a calcite standard (calcite from Helgustadir in Iceland). The CL recording system consists of an EG&G^{TM} digital triple grating spectrograph with a liquid N_2-cooled CCD camera. For optimisation of the signal to noise ratio the CCD camera was cooled down to $-120 \pm 0.5\,^{\circ}C$. The spectra were accumulated for 5–30 s depending on CL-intensity. The analysed area was focussed to a spot of 30 µm in diameter. To prevent charging during irradiation the samples were coated with a thin film (5–10 nm) of gold. CL-spectrometry can be used to obtain quantitative analyses of Mn^{2+}. The quantitative CL spectral analysis is calibrated by using PIXE. In order to compare the quantitative CL detection limits with those of PIXE the same criterion for distinguishing a peak from background is applied. The minimum acceptable CL-peak is assumed to be $3/N_b$ (where N_b is the background at the peak high) (*Homman* et al., 1994). A detailed description of quantitative spectral analysis of CL can be found in *Habermann* (1997).

Electron Paramagnetic Resonance (EPR) measurements of carbonates and feldspar were carried out at room temperature at X-band frequencies of ~ 9.75 GHz with a Bruker ESP 300e spectrometer using 100 kHz modulation. The resonance frequency was determined by a frequency counter, and the magnetic field was calibrated using DPPH (α-diphenyl-β-picryl hydrazyl), which has a g-value of 2.0036 ± 0.0003. μ-PIXE analyses were made at the Bochum Dynamitron Tandem Laboratory (DTL) microprobe facility. A 3 MeV proton beam was focussed to about 10 µm in diameter and a beam current of 1–10 nA was used. The characteristic X-rays were detected with a Röntec® Si(Li) detector with an energy resolution of ~ 135 eV at 5.2 keV emitted X-ray energy. The detection limit for most of the transition metal elements is 1–10 ppm. Details of the experimental set-up and calibration of the analysis system are given in *Meijer* et al. (1994). The PIXE-spectra were analysed using the GUPIX software package (*Maxwell* et al., 1995).

REE-doped calcite samples were synthesised from solution at room temperature using the experimental set-up of *ten Have* and *Heijen* (1985). The Sm- and Eu-chloride concentrations in the solution are 150 mg dm^{-3} and ($SmCl_3$) 231 mg dm^{-3} ($EuCl_3$) respectively. Clear transparent calcite crystals, white spheres of aragonite and/or vaterite crystals were formed. CL- and micro-PIXE-measurements were carried out on the calcite crystals. Thin sections were analysed by CL-microscopy and spectroscopy and μ-PIXE, while single crystals and powder samples were used for EPR measurements.

CL-spectra

Quenching of intrinsic CL

In calcite, a broad intrinsic emission with peaks centred at 420 nm (e.g. *Calderón* et al., 1984) and 580 nm is most likely produced by intrinsic transitions related to the crystal, and is not related to impurities. The emission at 420 nm is most probably due to a self-trapped exciton (e.g. *Calderón* et al., 1984), while the emission at 580 nm is possibly attributed to structural defects like oxygen vacancies and broken Ca–O bonds (*Habermann* et al., 2000). The intensity of this emission is not only controlled by the intrinsic defect concentration but is also influenced by extrinsic defects, which can quench parts of the intrinsic CL by providing competitive recombination pathways. Particularly Fe^{2+} (which is not solely a quencher of extrinsic CL) can quench intrinsic CL efficiently. Figure 1 shows the quenched

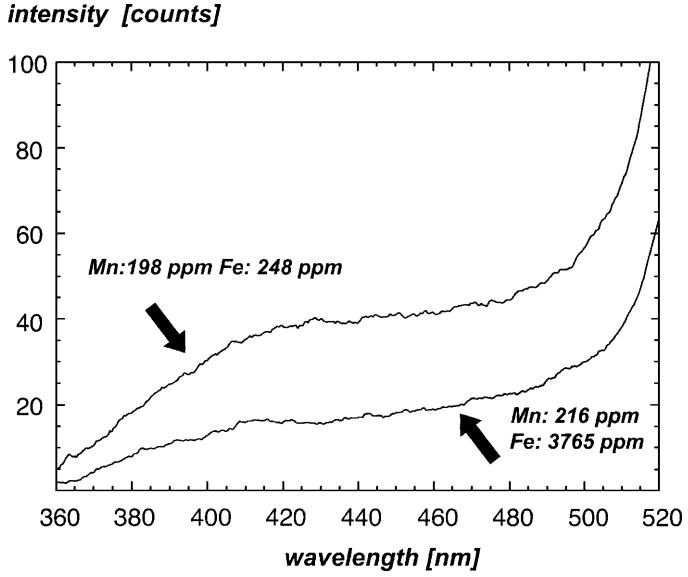

Fig. 1. CL-spectra of calcite with unquenched and quenched intrinsic bands by high Fe-concentration. The trace elements are analysed by micro-PIXE. The CL-spectra are recorded under same conditions (exposure time: 30 s, acceleration voltage: 15 kV, beam current density: 9 µA mm^{-2}) (samples: Iceland spar calcite; Mn 198 ppm, Fe 248 ppm: calcite from a Triassic limestone; Mn 216 ppm, Fe 3765 ppm)

intrinsic CL of calcite at high Fe-concentrations. It should be noted that this quenching could be used as an indicator of high Fe levels.

Line-shape, self-quenching and cluster structures

Self-quenching (concentration quenching) results from multipole energy transfer between ions of the same kind and takes place at high activator concentrations (*Marfunin*, 1979). At low activator concentrations, when the average spacing between the activator ions is large, this process is very weak (*Marshall*, 1988). The critical concentration at which self-quenching becomes efficient is different for each type of the activator and their specific transitions, and also depends on the host crystal structure. For example, photoluminescence (PL) data of Pr^{3+}-doped YPO_4 show that the intensity of the emission originating from $^3P_0$ and $^1D_2$ levels is different as their concentration changes (*Chen* et al., 2001). PL data from REE-activated scheelite place the starting level of self-quenching at ~ 10 ppm (*Kempe* et al., 1991). Higher critical concentrations (500–1000 ppm) are documented for Mn^{2+}-activated CL in the calcite structure (*Mason*, 1987; *El Ali* et al., 1993; *Habermann* et al., 2000).

Another consequence of a high concentration of activator elements is the possible formation of cluster structures. Figure 2a shows two CL-spectra of ''Iceland spar'' calcite with 90 and 5342 ppm Mn^{2+} respectively. Calcite with a high Mn^{2+} concentration is characterised by a broader Mn^{2+}-peak and a slight shift of the peak maximum to lower wavelengths. These effects can be explained by changes in the local crystal field and/or the formation of cluster structures. EPR measurements support this interpretation as the extreme expansion of the Mn^{2+} EPR line widths cannot be solely explained by dipole–dipole interactions (Fig. 2b). The formation of Mn^{2+} dominated cluster structures and slight changes of the symmetry in cluster and host crystal structures might be additional effects. To investigate such cluster structures it is very efficient to use elements such as Mn^{2+} and Fe^{3+} as probes of atomic scale. The crystal structures and crystal field influence the energy level of the transitions of these elements so much that the energy of emission is a sensitive signal of slight changes in the local crystal field and structure. It should be noted that the full width of the peak at half maximum (FWHM) also increases when the Mg-content of calcite is >0.8 mol% although the Mn and Fe concentration is <1000 ppm respectively. This excludes Mn- and/or Fe-clustering as a reason for the broadening of the Mn^{2+} peak and only Mn^{2+} activated emission composed of two peaks remains a possible explanation (Fig. 3a) (*Habermann*, 1997). The first peak position (615 nm) belongs to a Mg-free calcite structure where the crystal field splitting parameter Δ for the Mg-free calcite $\Delta = 7100 \pm 200\,cm^{-1}$ (Δ value from *Walker* et al., 1989). The second peak position (654 nm) seems to be related to Mg-dominated cluster structures with a $\Delta \sim 8450 \pm 200\,cm^{-1}$, which is close to the value of magnesite (*Habermann*, 1997), and Mn^{2+} at the Mg-site in dolomite (*El Ali* et al., 1993).

Biogenic and low temperature synthetic Mg-calcites show no evidence of dolomite cation ordering (e.g. *Mackenzie* et al., 1983), but in high-temperature Mg-calcite dolomite cation ordering is documented (e.g. *Khan* and *Barber*, 1990). The Mn^{2+} emission can be composed of superposed peaks related to Mn^{2+}

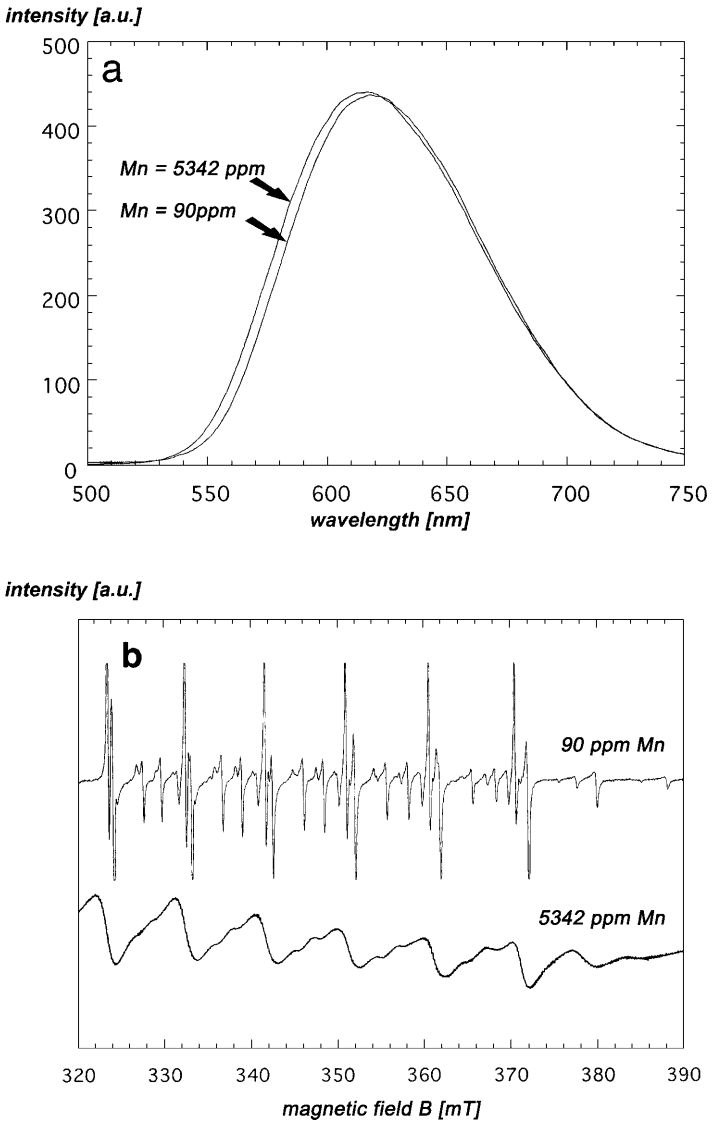

Fig. 2. **a** Normalised CL-spectra of Mn^{2+}-activated "Iceland spar" calcite with 90 ppm and 5342 ppm Mn. The high Mn^{2+} concentration causes a broadening of the Mn^{2+} CL-peak on the low wavelength side and a shift of the peak towards higher energy. **b** First derivatives of EPR-powder spectra of Mn^{2+}-activated calcite. The narrow structure of the lines of the sample with 90 ppm Mn is a characteristic of "Iceland spar" calcite. Less perfection of the crystallographic order, cluster structures and dipole–dipole interactions are causes for the extreme broadening of the EPR-lines

incorporated in different kinds of domains and host crystal structures. In the case of biogenic and low-temperature Mg-calcite, the wavelength of Mn^{2+} related emission is based on the superposition of two peaks. However, a CL-spectrum of other carbonates with complex microstructure and crystal structure can be composed of more than two Mn^{2+}-peaks.

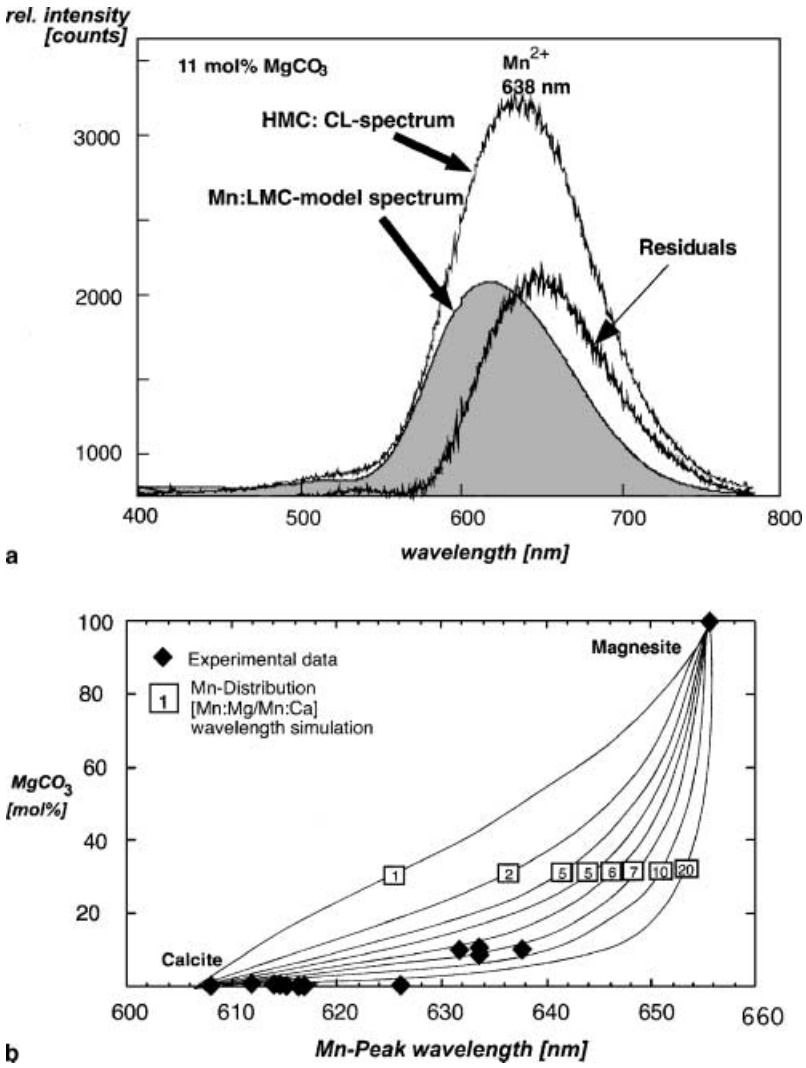

Fig. 3. **a** Spectrum of Mn^{2+} activated CL of a Mg-calcite (echinoderm skeleton) with 11 mol% $MgCO_3$. The peak position of 632 nm and FWHM of 100 nm are both higher than assumed for one Mn^{2+} peak. Subtracting the model spectrum of Mn^{2+}:$CaCO_3$ clearly shows the occurrence of a second Mn^{2+}-peak related to a Mn^{2+}:$MgCO_3$-cluster structure. **b** Relation between experimental data (calcite from biogenic and sedimentary origin and magnesite of metamorphic origin) and results from a simulation of the wavelength of Mn^{2+}-activated CL and the content of calcite. The simulation based on the calculation of the Mn^{2+} incorporation in Ca- and Mg-lattice positions at different Mn^{2+}-distribution quotients (>1) and constant absolute Mn^{2+}-concentration

Simulations of the relationship between Mn^{2+} distribution and emission wavelength with experimental data from biogenic and low-temperature calcite are plotted in Fig. 3b. There is no linear correlation between the Mn^{2+}-peak wavelength and the Mg-content of calcite as described by *Sommer* (1972) and *Koberski* (1992). Additionally, the maximum CL intensity is not linearly correlated with the integral intensity of both Mn^{2+}-peaks. A fitting procedure is clearly needed to

estimate the Mn^{2+}-partitioning between the crystal and the cluster structures. High Resolution Transmission Electron Microscope (HRTEM) analyses by *Khan* and *Barber* (1990) show at ~ 1 mol% $MgCO_3$ the first occurrence of ''ribbon microstructures'' in Mg-calcite from the oxidised zone of an ore body. At the same concentration level of $MgCO_3$ in low-temperature Mg-calcite the increase of the FWHM of the Mn^{2+} related CL starts (*Habermann* et al., 2000). Both CL-spectroscopy and HRTEM experiments reveal that Mg^{2+} is not homogeneously distributed and three-dimensional $MgCO_3$ clustering might occur in Mg-calcite. X-ray diffraction (XRD) data from an echinoderm skeleton, in which a homogeneous Mg-distribution and a continuous decrease of the Ca–O distance with increasing Mg-content is assumed (*Althoff*, 1977), contradict the CL data of echinoderm skeletons (*Habermann* et al., 2000).

Correlation between CL intensity and trace element concentration

Manganese in calcite and feldspar

A linear correlation between the Mn concentration and the CL-intensity in calcite and feldspar (see also *Mora* and *Ramseyer*, 1992) is documented in Fig. 4. Mn^{2+} concentration quenching and quenching by Fe^{2+} give rise to deviations from the linear correlation in calcite, if the concentration of Mn^{2+} is >1000 ppm and the concentration of Fe^{2+} is >3000 ppm (Fig. 4c). Thus, Mn^{2+} concentration quenching seems to be more effective than quenching by Fe^{2+} (*Habermann*, 1997). The efficiency of ''Fe-quenching'' increases with increasing Mn^{2+} content according to the decreasing average Fe^{2+} and Mn^{2+} distances in the crystal (*Habermann* et al., 2000). Other quencher ions like Ni^{2+} are much less effective than Fe^{2+} (*Marfunin*, 1979) and only important at high concentrations, easily detectable by conventional EPMA.

Figure 5 shows the comparison between results from quantitative analyses of Mn^{2+}-activated CL and μ-PIXE analyses (*Habermann* et al., 2000). Deviations from an ideal correlation are mainly based on small variations in the Mn distribution, the statistic error of the methods used, differences in the analysed spot size (μ-PIXE 10 μm; CL 30 μm), slight inhomogeneities of the element distribution, and the variable depth of penetration (μ-PIXE 50 μm; CL ~ 2–5 μm).

REE-doped synthetic calcite

Most divalent and trivalent REE show CL-emission in the near UV, visible and IR regions of the electromagnetic spectrum. REE incorporated in calcite, feldspar, fluorite and apatite are unequivocally detectable using CL-spectroscopy (*Blanc* et al., 2000). The REE are mostly incorporated in natural minerals as the whole group of elements where sensitising and quenching by other REE are important effects, yielding strong variations in the correlation between REE-activated CL-intensities and REE-concentrations. Not all transitions of the REE are affected in the same way by quenching and sensitising processes. Therefore only specific transitions are suitable for quantitative measurements. Figure 6 shows the fit of the CL-spectrum of a natural REE-containing calcite, based on the data from single

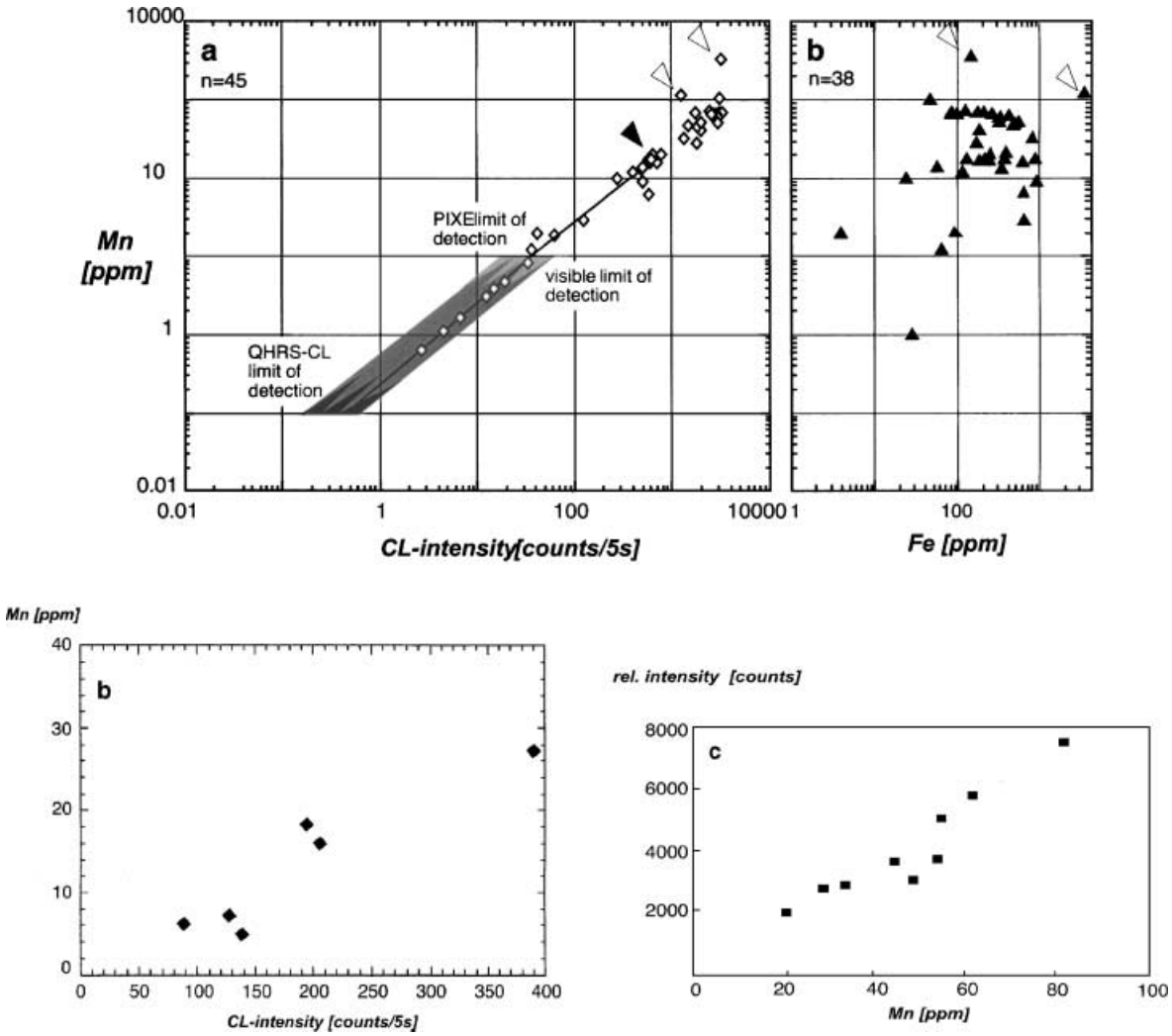

Fig. 4. **a** Correlation between CL-intensity (normalised to counts/5 s), Mn- and Fe-content in visually homogeneously luminescent calcite. The data reveal an excellent linear correlation (R = 0.97) in the range of 19–1000 ppm. Mn-analyses below the LOD of μ-PIXE ($\sim$ 10 ppm) were done using Quantitative High Resolution Spectroscopy of CL (QHRS-CL) (*Habermann* et al., 1999). The calibration value (linear function) of QHRS-CL based on the analysis data of an ''Iceland spar'' calcite (black arrow). Two analyses points show a distinct deviation from that linear correlation indicating that Fe^{2+}-quenching and Mn^{2+}-concentration-quenching occur at $\sim$ 4000 ppm and $\sim$ 1100 ppm respectively (white arrows) (modified after *Habermann* et al., 1999). **b** Correlation between CL-intensity (normalised to counts/5 s) and Mn-content in a plagioclase crystal. The data reveal a linear correlation in the range between 4.8–27.2 ppm. The μ-PIXE analyses at 4.8 and 7.3 ppm are only twice above the LOD of μ-PIXE (modified from *Habermann* et al., 1999). **c** Comparable data from *Götze* et al. (2000) for plagioclase crystals (modified after *Götze* et al., 2000)

REE-doped synthetic calcite crystals. Some of the lines, which are indicated in the residual spectrum, correspond to sensitised and quenched transitions. Combined μ-PIXE and CL-spectroscopy analyses of Sm- and Eu-doped synthetic

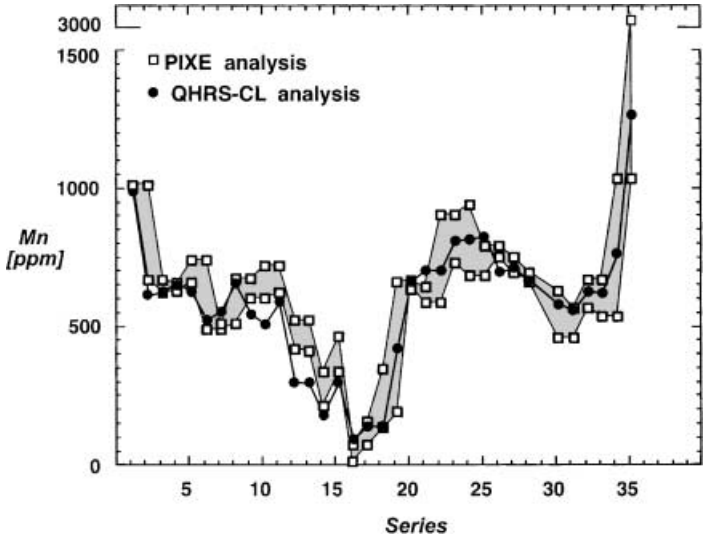

Fig. 5. Comparison between line-scan results of μ-PIXE and QHRS-CL analyses of the Mn concentration in calcite (modified from *Habermann* et al., 2000). QHRS-CL analysis areas are mostly located between the PIXE analysis spots. Deviations are chiefly caused by small inhomogeneities in the Mn-distribution, different spot area of micro-PIXE (10–15 µm) and QHRS-CL (30 µm) and analysis charge

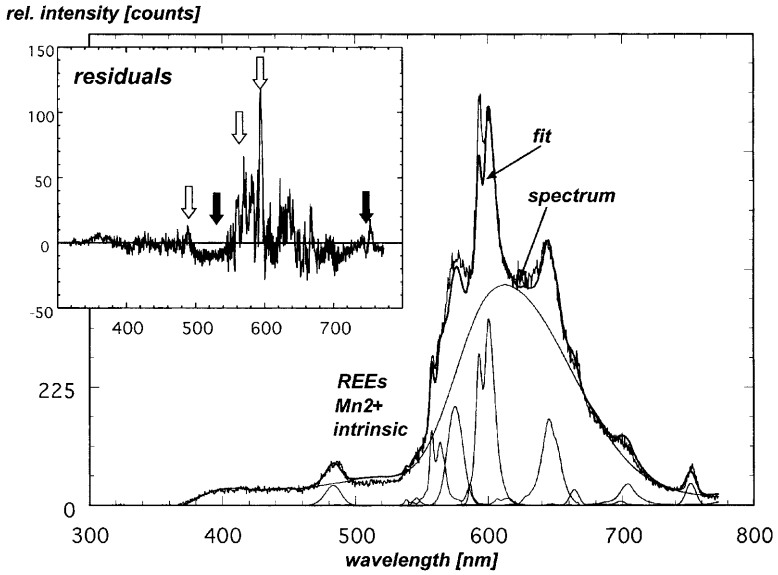

Fig. 6. CL-spectrum and fit of a natural REE-containing calcite. The data of the fit are based on single REE-doped synthetic calcite, Mn^{2+}-activated "Iceland spar" calcite and pure blue luminescent sinter calcite. Sensitising and quenching of different REE-transitions are documented in the residuals, there white arrows marked some sensitised and black arrows indicate quenched transitions and quenched intrinsic luminescence, respectively

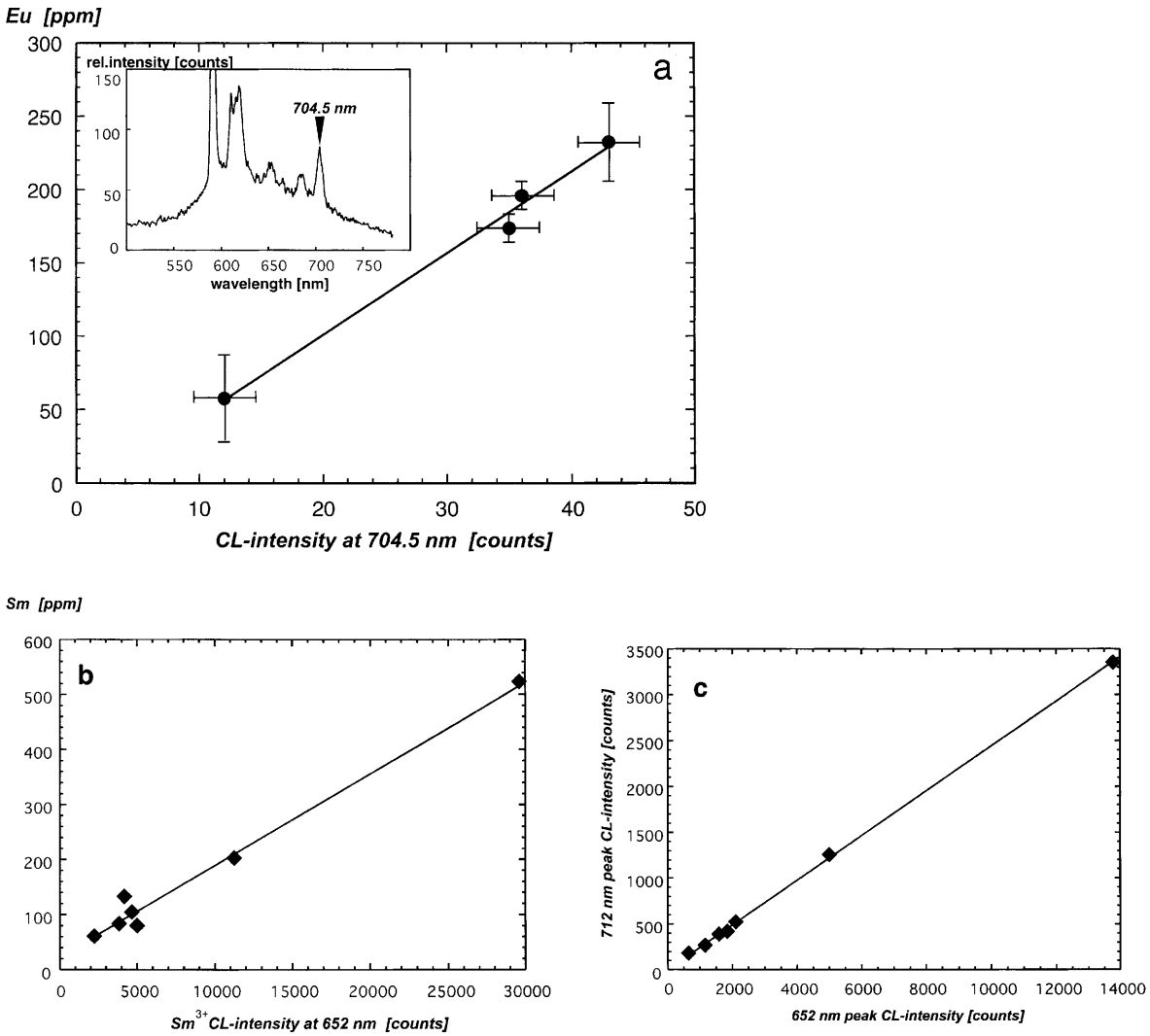

Fig. 7. **a**, **b** Correlation between Sm and Eu concentration and CL-intensity of synthetic REE-doped calcite. Analysed transitions: Sm^{3+}: $^4G_{5/2} \rightarrow {}^6H_{9/2}$ (at 652 nm); Eu^{3+}: $^5D_0 \rightarrow {}^7F_4$ (704.5 nm). **c** Correlation between the intensities of the 652 nm (transition: $^4G_{5/2} \rightarrow {}^6H_{9/2}$) and the 712 nm (transition: $^4G_{5/2} \rightarrow {}^6H_{11/2}$) Sm^{3+}-lines indicates that the analytical lines from the $^4G_{5/2} \rightarrow {}^6H_{9/2}$ transition is not underlain by Sm^{2+}-lines (transition: $^5D_0 \rightarrow {}^7F_2$)

calcite (Fig. 7a, b) suggest a linear correlation between the Sm^{3+}- and Eu^{3+}-activated CL intensity and the Sm- and Eu-concentration. However, the incorporation of divalent REE in the mineral structure is a limiting factor, because of different transition-probabilities of the REE^{2+} and REE^{3+} related transitions. These depend on the energy of excitation and the host crystal structure (*Mikhail* et al., 2001). However, in the CL- and EPR-spectra of Eu-doped calcite, no indication of divalent Eu has been detected. As the Sm-doped crystals were synthesised under the same conditions divalent Sm is not expected in the calcite structure. There is also no evidence in the CL-spectra that the intensity of the Sm^{3+} line

(transition: $^4G_{5/2} \rightarrow {}^6H_{11/2}$) is underlain by a Sm^{2+} line ($^5D_0 \rightarrow {}^7F_2$). This is supported by the linear correlation of the intensities of the 652 nm ($^4G_{5/2} \rightarrow {}^6H_{9/2}$) and the 712 nm ($^4G_{5/2} \rightarrow {}^6H_{11/2}$) Sm^{3+}-lines (Fig. 7c).

CL-spectroscopy can measure REE concentrations below the detection limit of methods such as μ-PIXE, which lie often $\sim$ 10–20 ppm. Although this limitation is important for calibrating the quantitative CL-spectroscopy, the data indicate that in special cases (semi-)quantitative REE analyses by CL-spectroscopy is possible and is an appropriate extension of other forms of analysis.

Conclusions

The linear correlation of Mn^{2+}-, Sm^{3+}- and Eu^{3+}-activated CL in calcite suggests that quantitative CL-spectroscopy is possible. For Mn^{2+} in calcite quantitative CL is limited to the concentration range of ppb up to $\sim 10^3$ ppm. The conspicuous potential of this method lies not only in the direct compositional information within the spectra, but also in the numerous and complex information embedded in the CL-spectrum, including information on the crystal field, cluster- and hetero-structures of minerals, lattice position of spin centres and the charge of activator ions. However, the limitations of quantitative CL are mainly defined by the complexity of sensitising, quenching effects and the complex structure of the CL-spectra of natural minerals. Another limitation is *the problem of calibration and standards*. Because of the high sensitivity of CL only a few methods like μ-PIXE, Laser Ablation Inductively Coupled Plasma Mass Spectrometry (LA-ICPMS) and Secondary Ion Mass Spectrometry (SIMS) are suitable for calibration and this has to be done for each mineral structure separately. The efficiency of the combination of quantitative CL-spectroscopy and sensitive trace element analyses applied to problems in material sciences and geosciences might be an important future application of CL-spectroscopy.

Acknowledgements

I thank *D. K. Richter, J. R. Niklas, R. D. Neuser, J. Götze, T. Götte, A. Stephan* and *J. Meyer* for their kind co-operation with the investigations and many helpful discussions. The author is grateful to *K. Ramseyer*, *A. Finch* and an anonymous referee for constructive criticism and many useful comments on the initial version of the manuscript.

References

Althoff PL (1977) Structural refinement of dolomite and a magnesian calcite and implications for dolomite formation in the marine environment. Am Mineral 62: 772–783

Blanc P, Baumer A, Cesborn F, Ohnenstetter D, Panczer G, Rémond G (2000) Systematic cathodoluminescence spectral analysis of synthetic doped minerals: anhydrite, apatite, calcite, fluorite, scheelite and zircon. In: *Pagel* et al. (eds) Cathodoluminescence in geosciences. Springer, Berlin Heidelberg New York Tokyo, pp 127–160

Calderón T, Aguilar M, Jaque F, Coy-Yll R (1984) Thermoluminescence from natural calcite. J Phys 17: 2077–2038

Chen X, Luo Z, Jaque D, Romero JJ, Sole JG, Huang Y, Jiang A, Tu C (2001) Comparision of optical spectra of Nd^{3+} in $NdAl_3(BO_3)_4$ (NAB), $Nd{:}GdAl_3(BO_3)_4$ (NGAB), and $Nd{:}Gd_{0.2}Y_{0.8}Al_3(BO_3)_4$ (NGYAB) crystals. J Phys Condens Matter 13: 1171–1178

Frank D, Carpenter AB, Oglesby TW (1982) Cathodoluminescence and composition of calcite cement in the Taum Sauk limestone (Upper Cambrian), SE Missouri. J Sediment Petrol 52: 631–638

Götze J, Krbetschek MR, Habermann D, Wolf D (2000) High resolution cathodoluminescence studies of feldspar minerals. In: *Pagel* et al. (eds) Cathodoluminescence in geosciences. Springer, Berlin Heidelberg New York Tokyo, pp 246–270

Habermann D (1997) Quantitative hochauflösende Kathodolumineszenz-Spectroskopie von Calcit und Dolomit. Thesis, Ruhr-Universität Bochum, Germany, 172 pp

Habermann D, Meijer J, Neuser RD, Richter DK, Rolfs C, Stephan A (1999) Micro-PIXE and quantitative cathodoluminescence spectroscopy: combined high resolution trace element analyses in minerals. Nucl Instr Meth Phys Res B150: 470–477

Habermann D, Neuser RD, Richter DK (2000) Quantitative high resolution spectral analysis of Mn^{2+} in sedimentary calcite. In: *Pagel* et al. (eds) Cathodoluminescence in geosciences. Springer, Berlin Heidelberg New York Tokyo, pp 331–358

Hemming NG, Meyers WJ, Grams JC (1989) Cathodoluminescence in diagenetic calcites: the role of Fe and Mn as deduced from electron probe and spectrophotometric measurements. J Sediment Petrol 59: 404–411

Homman NP, Yang C, Malmqvist KG (1994) A highly sensitive method for rare-earth element analysis using ionoluminescence combined with PIXE. Nucl Instr Meth Phys Res A353: 610–614

Kempe U, Trinkler M, Wolf D (1991) Yttrium und Seltenerdfotolumineszenz natürlicher Scheelite. Chem Erde 51: 275–289

Khan MR, Barber DJ (1990) Compositional-related microstructures in zinc-bearing carbonate assemblages from Broken Hill, New South Wales. Mineral Petrol 41: 229–245

Koberski U (1992) Anwendung der Kathodolumineszenz auf Fragestellungen in der Petrologie. Thesis, Albert-Universität Freiburg, Germany, 213 pp

Marfunin AS (1979) Spectroscopy, luminescence and radiation centres in minerals. Springer, Berlin Heidelberg, 352 pp

Marshall DJ (1988) Cathodoluminescence of geological materials. Unwin-Hyman, Boston, 146 pp

Mason RA (1987) Ion microprobe analysis of trace elements in calcite with an application to the cathodoluminescence zonation of limestone cements from the Lower Carboniferous of South Wales, U.K. Chem Geol 64: 209–224

Maxwell JA, Teesdale WJ, Campbell JL (1995) The Guelph PIXE software package II. Nucl Instr Meth Phys Res B95: 407–421

Meijer J, Stephan A, Adamczewski J, Bukow HH, Rolfs C, Pickart T, Bruhn F, Veizer J (1994) PIXE microprobe for geoscience applications. Nucl Instr Meth Phys Res B89: 229–232

Mackenzie FT, Bishop WD, Bishop FC, Loijens J, Schoonmaker J, Wollast R (1983) Magnesian calcites: low-temperature occurrence, solubility and solid solution behavior. Rev Mineral 11: 97–144

Mikhail P, Hulliger J, Ramseyer K (2001) Can cathodoluminescence or photoluminescence determine the valence states of samarium? Cathodoluminescence in Geosciences (CL 2001), Abstracts, pp 86–87

Mora CI, Ramseyer K (1992) Cathodoluminescence of coexisting plagioclase, Boehls Buttle anorthosite: CL activators and fluid flow paths. Am Mineral 77: 1258–1265

Neuser RD (1995) A new high-intensity cathodoluminescence microscope and its application to weakly luminescing minerals. Bochumer geol geotech Arb 44: 116–118

Ramseyer K, Fisher J, Matter A, Eberhardt P, Geiss J (1989) A cathodoluminescence microscope for low intensity luminescence. J Sediment Petrol 59: 619–622

Richter DK, Zinkernagel U (1981) Zur Anwendung der Kathodolumineszenz in der Karbonatpetrographie. Geol Rundsch 70: 1276–1302

Sommer SE (1972a) Cathodoluminescence of carbonates. 1. Characterisation of cathodoluminescence from carbonate solid solutions. Chem Geol 9: 257–273

Telfer DJ, Walker G (1978) Ligand field bands of Mn^{2+} and Fe^{3+} luminescence centres and their site occupancy in plagioclase feldspars. Mod Geol 6: 199–210

ten Have T, Heijnen W (1985) Cathodoluminescence activation and zonation in carbonate rocks: an experimental approach. Geologie en Mijnbouw 64: 297–310

Walker G, Abumere OE, Kamaluddin B (1989) Luminescence spectroscopy of Mn^{2+} centers in rock-forming carbonates. Mineral Mag 53: 201–211

Yacobi BG, Holt DB (1990) Cathodoluminescence microscopy of inorganic solids. Plenum, New York, 292 pp

Author's address: *D. Habermann*, Institute of Experimental Physics, University of Technology Freiberg, Silbermannstrasse 1, D-09596 Freiberg, Germany, e-mail: dirk.habermann@rena.de